Letter

Nonsymmorphic Luttinger liquids in generalized antiferromagnetic Kitaev spin-$\frac{1}{2}$ chains

Wang Yang [1,*] Chao Xu [2,*] Shenglong Xu,[3] Alberto Nocera [4] and Ian Affleck[4]

[1]*School of Physics, Nankai University, Tianjin 300071, China*

[2]*Kavli Institute for Theoretical Sciences, University of Chinese Academy of Sciences, Beijing 100190, China*

[3]*Department of Physics and Astronomy, Texas A&M University, College Station, Texas 77843, USA*

[4]*Department of Physics and Astronomy and Stewart Blusson Quantum Matter Institute, University of British Columbia,
Vancouver, British Columbia, Canada V6T 1Z1*

We perform a detailed study on the consequences of the nonsymmorphic symmetries in the Luttinger phase of the one-dimensional (1D) spin-$\frac{1}{2}$ Kitaev-Heisenberg-Gamma model with an antiferromagnetic Kitaev interaction. Although the low-energy Hamiltonian has an emergent U(1) symmetry, the bosonization formulas for the spin operators contain ten nonuniversal coefficients which only respect the discrete nonsymmorphic symmetries and can be determined by our density matrix renormalization group simulations to a high degree of accuracy. Using the nonsymmorphic bosonization formulas, the response to weak magnetic field is analyzed, and the zigzag phase in the 2D Kitaev-Heisenberg-Gamma model is recovered by weakly coupling an infinite number of 1D chains. Furthermore, we find a line of critical points with an emergent SU(2)$_1$ conformal symmetry located on the boundary of the Luttinger liquid phase. Our work reveals the rich physics related to nonsymmorphic symmetries in strongly correlated quantum magnetic models, and demonstrates the usefulness of 1D analysis for understanding the 2D Kitaev physics.

Nonsymmorphic symmetries are symmetry operations involving a combination of rotations or reflections with translations, where the individual operations do not leave the system invariant on their own. Recently, there has been a surge of research interests in studying the roles played by the nonsymmorphic symmetries in noninteracting and weakly interacting condensed matter systems [1–12] including hourglass fermions, Dirac insulators, and topological semimetals, though the strongly interacting physics related to nonsymmorphic symmetries remain much less investigated [13,14].

The Kitaev materials on the two-dimensional (2D) honeycomb lattice have recently been under intense research attention in condensed matter physics [15–38], since they can potentially provide solid state realizations for the 2D Kitaev spin-$\frac{1}{2}$ model known as a platform for topological quantum computations [39,40]. The zigzag phase is among the earliest experimentally discovered magnetic phases in Kitaev materials, most of which have ferromagnetic (FM) Kitaev interactions, though the zigzag order is also predicted to exist in systems with antiferromagnetic (AFM) Kitaev interactions. On the other hand, 2D suffers analytical and numerical difficulties, which hinders a complete theoretical understanding of Kitaev materials. In view of this, a number of theoretical studies have been performed on one-dimensional (1D) Kitaev spin models [41–52], and the hope is that 1D studies can help understand the 2D physics.

In this Letter, we perform a detailed study on the consequences of the nonsymmorphic symmetry group in the spin-$\frac{1}{2}$

Kitaev-Heisenberg-Gamma ($KJ\Gamma$) chain with an AFM Kitaev interaction, and their implications to 2D physics. Our starting point is the observation of an extended Luttinger liquid phase in the AFM Kitaev region of the spin-$\frac{1}{2}$ $KJ\Gamma$ chain [45]. In this Letter, we find that while the nonsymmorphic symmetries are smeared out in the low-energy Luttinger liquid theory which has an emergent U(1) symmetry, they manifest themselves as ten nonuniversal coefficients in the bosonization formulas of the spin operators, leading to gapless spinon modes at $\pm\pi/2$ wave vectors in addition to 0 and π. Using density matrix renormalization group (DMRG) simulations, the bosonization coefficients are determined to a high degree of accuracy, which can be used to analytically calculate any low-energy property of the system.

As an application of the nonsymmorphic bosonization formulas, the response to weak magnetic fields is analyzed, and interestingly, regardless of the direction of the applied weak magnetic field, the system responds only along a particular fixed direction with the opening of a spin gap. In addition, an infinite number of weakly coupled $KJ\Gamma$ chains on the honeycomb lattice is studied. The mean-field Hamiltonian is obtained using the nonsymmorphic bosonization formulas and then solved in a self-consistent way, which recovers the zigzag phase in the 2D spin-$\frac{1}{2}$ $KJ\Gamma$ model. Finally, we reveal a line of critical points with an emergent SU(2)$_1$ conformal symmetry located on the boundary of the Luttinger liquid phase.

Model and symmetries. The 1D spin-$\frac{1}{2}$ $KJ\Gamma$ model is defined as

$$H = \sum_{\langle ij \rangle = \gamma} \left[K S_i^\gamma S_j^\gamma + J \vec{S}_i \cdot \vec{S}_j + \Gamma \left(S_i^\alpha S_j^\beta + S_i^\beta S_j^\alpha \right) \right], \quad (1)$$
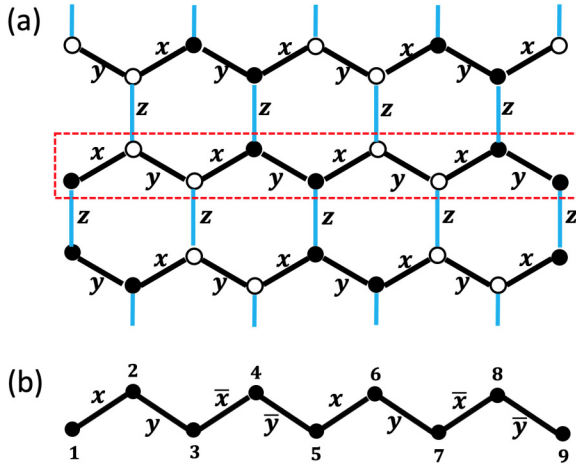
FIG. 1. (a) Zigzag order of the spin-$\frac{1}{2}$ dimerized $KJ\Gamma$ model on the honeycomb lattice; (b) bond pattern after the four-sublattice rotation for the chain in (a) enclosed by the red dashed line. In (a), the black and blue lines denote the strong and weak bonds; the solid and open circles represent the sites which have positive and negative components along the S^x direction, respectively.

in which γ is the spin direction associated with the bond between nearest-neighboring sites i and j, alternating between x and y as shown in Fig. 1(a); $\alpha \neq \beta$ are the two spin directions among x, y, z other than γ; and K, J, Γ are the Kitaev, Heisenberg, and Gamma couplings, respectively. The Hamiltonian in Eq. (1) is obtained by selecting out one row out of the 2D $KJ\Gamma$ model on the honeycomb lattice as shown in Fig. 1(a). We will consider the parameter region $K > 0, J < 0$. Since Γ changes sign under a global spin rotation around the z axis by π, there is the equivalence $(K, J, \Gamma) \simeq (K, J, -\Gamma)$, and we will take $\Gamma > 0$ for simplicity.

A useful transformation is the four-sublattice rotation U_4 [36,45], which leaves the spins on sites $4n$ ($n \in \mathbb{Z}$) unchanged, and acts as π rotations around the y, z, and x axes on sites $1 + 4n$, $2 + 4n$, and $3 + 4n$, respectively. The transformed Hamiltonian acquires the following form,

$$H' = \sum_{\langle ij \rangle} \left[K'S_i^\gamma S_j^\gamma - J\vec{S}_i \cdot \vec{S}_j + \epsilon(\gamma)\Gamma \left(S_i^\alpha S_j^\beta + S_i^\beta S_j^\alpha \right) \right], \quad (2)$$

in which $K' = K + 2J$; the bond pattern for $\gamma \in \{x, y, \bar{x}, \bar{y}\}$ is shown in Fig. 1(b); $S_j^{\bar{\gamma}} = S_j^\gamma$; $\alpha \neq \beta$ are the two spin directions different from γ; and $\epsilon(x) = \epsilon(y) = -\epsilon(\bar{x}) = -\epsilon(\bar{y}) = 1$. The advantage of U_4 is that it reveals a hidden SU(2) symmetric AFM point at $J = -K/2$, $\Gamma = 0$, which provides a perturbative starting point to analyze the parameter region nearby [36,45]. Unless otherwise stated, we carry out the analysis within the four-sublattice rotated frame henceforth.

We first briefly discuss the symmetries of H' in Eq. (2) [45]. The symmetry group G of H' is generated by time-reversal symmetry T, screw operation $R(\hat{z}, -\pi/2)T_a$, and composite operation $R(\hat{y}, \pi)I$, where a is the lattice constant, T_{na} is the translation operator by n lattice sites, I is the spatial inversion with respect to the bond center between sites 2 and 3, and $R(\hat{n}, \phi)$ represents a global spin rotation around the $\hat{n}$ direction by an angle ϕ. The group structure of G is $G/\langle T_{4a} \rangle \cong D_{4d}$ in which $\langle \cdots \rangle$ is the group generated by the

elements within the brackets, and $D_{4d} \cong D_4 \times \mathbb{Z}_2^T$, where D_4 is the dihedral group of order eight and $\mathbb{Z}_2^T$ is the $\mathbb{Z}_2$ group generated by T [for more details, see Sec. II in Supplemental Material (SM) [53]].

The phase diagram in the $K > 0$, $J < 0$ region is shown in Fig. 2(a) [45], in which the horizontal axis ψ is defined by $K = \cos(\psi)$, $\Gamma = \sin(\psi)$. We will mainly focus on the Luttinger liquid phase [denoted as "LL" in Fig. 2(a)] in this Letter. When $K' > 0$ and $\Gamma \neq 0$, at low energies, the K' term in H' contributes to an easy-plane anisotropy whereas the Γ term cancels to leading order since the differences between neighboring sites are smeared out in the long-distance limit, which provides an intuitive explanation for the origin of the Luttinger liquid phase.

Nonsymmorphic bosonization formulas. In the Luttinger liquid phase, the low-energy physics is described by the Luttinger liquid Hamiltonian [54,55] $H_{LL} = \frac{v}{2} \int dx [\kappa^{-1}(\nabla\varphi)^2 + \kappa(\nabla\theta)^2]$, in which v is the velocity, κ is the Luttinger parameter, and the θ, φ fields satisfy the commutation relation $[\varphi(x), \theta(x')] = \frac{i}{2}\text{sgn}(x' - x)$. We derive the bosonization formulas which are consistent with the nonsymmorphic symmetry group of the system. In general, the spin operators can be related to the low-energy fields as

$$S_{j+4n}^\alpha = D_{\alpha\beta}^{(j)} J^\beta(x) + (-)^j C_{\alpha\beta}^{(j)} N^\beta(x), \quad (3)$$

in which $\alpha, \beta = x, y, z$; $1 \leqslant j \leqslant 4$; $x = (j + 4n)a$; $D^{(j)}, C^{(j)}$ are 3×3 matrices; the smeared spin densities J^α, N^α ($\alpha = x, y, z$) are given by $J^\pm = \frac{2}{a}\cos(\sqrt{4\pi}\varphi)e^{\pm i\sqrt{\pi}\theta}$, $J^z = -\sqrt{2}\pi\nabla\varphi$, $N^\pm = \frac{\sqrt{2}}{a}e^{\pm i\sqrt{\pi}\theta}$, $N^z = \frac{\sqrt{2}}{a}\sin(\sqrt{4\pi}\varphi)$, where $J^\pm = J^x \pm iJ^y$ and $N^\pm = N^x \pm iN^y$ [56]. The invariance under the symmetries $R(\hat{z}, -\pi/2)T_a$ and $R(\hat{y}, \pi)I$ requires

$$\Lambda^{(j+1)} = R_z\Lambda^{(j)}(R_z)^{-1}, \quad \Lambda^{(5-j)} = R_y\Lambda^{(j)}(R_y)^{-1}, \quad (4)$$

in which $\Lambda = C, D$; $j = 5$ is understood as 1 (modulo 4); and R_z and R_y are the 3×3 rotation matrices corresponding to $R(\hat{z}, -\pi/2)$ and $R(\hat{y}, \pi)$, respectively. The solution of Eq. (4)
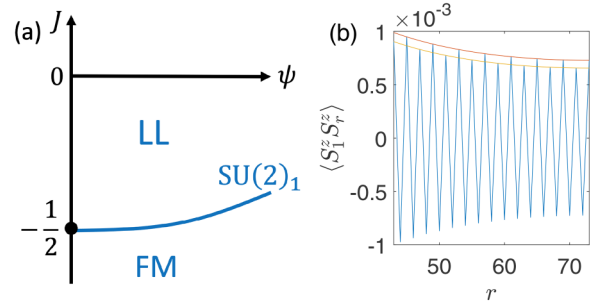

FIG. 2. (a) Phase diagram of the spin-$\frac{1}{2}$ $KJ\Gamma$ chain in the region $K > 0, J < 0$, in which the vertical axis is J and the horizontal axis is ψ where $K = \cos(\psi)$ and $\Gamma = \sin(\psi)$; (b) $\langle S_1^z S_r^z \rangle$ as a function of r. In (a), "LL," "FM," and "SU(2)$_1$" denote the Luttinger liquid phase, the FM phase, and the line of points with emergent SU(2)$_1$ conformal symmetry, respectively. In (b), DMRG numerics are performed for $K' = 1, J = -1, \Gamma = 0.35$ in Eq. (2) on a system of $L = 144$ sites with periodic boundary conditions.

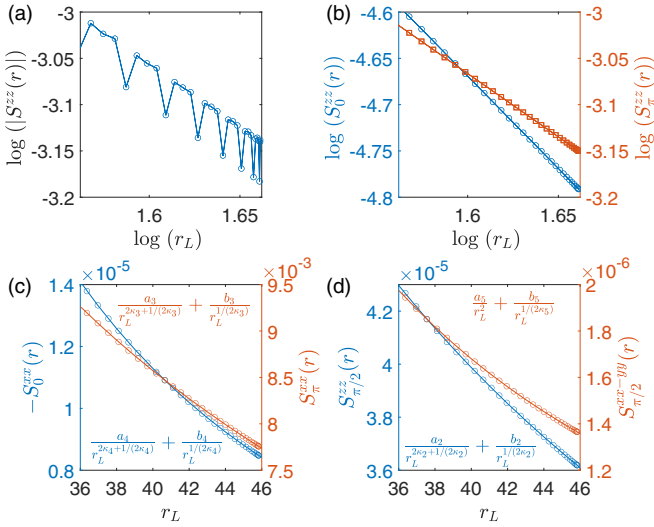|	$|a_\Lambda|$	$|i_\Lambda|$	$|c_\Lambda|$	$|h_\Lambda|$	$|b_\Lambda|$
$\Lambda = C$	0.129	0.363	0.0244	0.0138	0.00103
$\Lambda = D$	0.161	0.182	0.0359	0.0266	?

FIG. 3. (a) $|S^{zz}(r)|$ as a function of $r_L = L/\pi \sin(\pi r/L)$ on a log-log scale where $S^{zz}(r) = \langle S_1^z S_{1+r}^z \rangle$; (b) fits of $-S_0^{zz}(r)$ (blue) and $S_\pi^{zz}(r)$ (orange) as functions of r_L on a log-log scale using linear relations; (c) fits of $-S_0^{xx}(r)$ (blue) and $S_\pi^{xx}(r)$ (orange); (d) fits of $S_{\pi/2}^{zz}$ (blue) and $S_{\pi/2}^{xx-yy}$ (orange). In (c) and (d), the functional forms used for the fits are shown. DMRG numerics are performed for $K' = 1$, $J = -1$, $\Gamma = 0.35$ in the four-sublattice rotated frame.

for Λ^1 ($\Lambda = C, D$) is

$$C^{(1)} = \begin{pmatrix} a_C & b_C & c_C \\ b_C & a_C & -c_C \\ h_C & -h_C & i_C \end{pmatrix},$$

$$D^{(1)} = \begin{pmatrix} a_D & b_D & c_D \\ b_D & a_D & -c_D \\ h_D & -h_D & i_D \end{pmatrix}, \qquad (5)$$

and the remaining matrices $C^{(j)}$, $D^{(j)}$ ($j = 2, 3, 4$) can be obtained from the relations in Eq. (4). We note that in contrast to the U(1) symmetric case, the bosonization formulas in Eq. (3) have low-energy spinon modes at $\pm\pi/2$ wave vectors in addition to zero and π wave vectors, and S_j^λ contains cross-directional components J^μ, N^μ where $\mu \neq \lambda$, not just diagonal ones.

Next, we discuss the numerical results for the spin correlation functions and fit the data with the nonsymmorphic bosonization formulas in Eq. (3) to determine the ten coefficients and the Luttinger parameter. DMRG simulations are performed in the four-sublattice rotated frame at a representative point in the Luttinger liquid phase with the parameters $K' = 1$, $J = -1$, $\Gamma = 0.35$, on a system of $L = 144$ sites using periodic boundary conditions [57].

Figure 2(b) displays $\langle S_1^z S_r^z \rangle$ as a function of r, which is dominated by the π-wave-vector oscillation; however, as can be seen from the data points guided by the red and orange lines, there exists a delicate subdominant structure having a four-site periodicity. Figure 3(a) shows $|\langle S_1^z S_{1+r}^z \rangle|$ as a function of r_L on a log-log scale, where $r_L = L/\pi \sin(\pi r/L)$ in accordance with conformal field theory in finite-size systems [55]. It can be clearly seen that Fig. 3(a) contains rugged oscillations in the data points, indicating an entangling of

different Fourier components, which hinders a high-precision determination of the critical exponent.

To study the spin correlation functions in more detail, we apply the nonsymmorphic bosonization formulas such that different Fourier components and decay powers can be disentangled. Notice that Eq. (3) predicts $\langle S_1^z S_{1+r}^z \rangle = S_0^{zz}(r) + (-)^{r-1} S_\pi^{zz}(r) - 2\cos[\frac{\pi}{2}(r + \frac{1}{2})] S_{\pi/2}^{zz}(r)$, where $S_0^{zz}(r) = -i_D^2 r^{-2}$, $S_\pi^{zz}(r) = i_C^2 r^{-2\kappa}$, and $S_{\pi/2}^{zz}(r) = c_C^2 r^{-1/(2\kappa)} - c_D^2 r^{-[2\kappa+1/(2\kappa)]}$. The blue and orange lines in Fig. 3(b) show the fits of $-S_0^{zz}$ and S_π^{zz} as a function of r_L on a log-log scale, respectively, using linear relations, where r is replaced by $r_L = L/\pi \sin(\pi r/L)$. The slope of the blue line is -1.995, very close to the predicted value of -2; the slope of the orange line yields a Luttinger parameter $\kappa_1 = 0.683$. The fit of $S_{\pi/2}^{zz}(r)$ using a functional form $a_2 r_L^{-1/(2\kappa_2)} + b_2 r_L^{-[2\kappa_2+1/(2\kappa_2)]}$ is shown as the blue line in Fig. 3(d) which gives $\kappa_2 = 0.685$. The extracted values of $|i_\Lambda|$ and $|c_\Lambda|$ ($\Lambda = C, D$) from Figs. 3(b) and 3(d) are included in Table I.

For the transverse correlations, Eq. (3) predicts the zero- and π-wave-vector oscillating components of $\langle S_1^x S_{1+r}^x \rangle$ to be $S_0^{xx}(r) = -a_D^2 r^{-2\kappa-1/(2\kappa)} + b_C^2/r^{-1/(2\kappa)}$ and $S_\pi^{xx}(r) = -b_D^2 r^{-2\kappa-1/(2\kappa)} + a_C^2 r^{1/(2\kappa)}$, respectively. The blue and orange lines in Fig. 3(c) show the fits of $-S_0^{xx}$ and S_π^{xx}, which give $\kappa_3 = 0.681$ from S_0^{xx}, and $\kappa_4 = 0.681$ from S_π^{xx}. In addition, Eq. (3) predicts the $\pm\pi/2$ component of $\langle S_1^x S_{1+r}^x \rangle - \langle S_1^y S_{1+r}^y \rangle$ to be $-\cos[\frac{\pi}{2}(r + \frac{1}{2})] S_{\pi/2}^{xx-yy}$ where $S_{\pi/2}^{xx-yy} = h_D^2 r^{-2} + h_C^2 r^{-2\kappa}$. The fit for $S_{\pi/2}^{xx-yy}$ is shown as the orange line in Fig. 3(d), giving $\kappa_5 = 0.682$. The extracted values of $|a_\Lambda|, |b_\Lambda|, |h_\Lambda|$ ($\Lambda = C, D$) from Figs. 3(c) and 3(d) are included in Table I, where the only exception is $|b_D|$. We note that the b_D term decays much faster than the a_C term, since the exponents are $2\kappa + 1/(2\kappa)$ for the former and $1/(2\kappa)$ for the latter. In addition, $|b_D|$ itself is much smaller than $|a_C|$. These two effects make it very difficult to extract a reliable value of $|b_D|$ since the b_D and a_C terms are mixed in $S_\pi^{xx}(r)$.

From the above discussions, we see that with the help of the proposed nonsymmorphic bosonization formulas, the fitting curves are rendered smooth without any ruggedness, and nearly all the bosonization coefficients are numerically determined which can be used to calculate any low-energy property of the system. In particular, different Fourier components of the correlation functions give five independently extracted values of Luttinger parameters, denoted as κ_i ($1 \leqslant i \leqslant 5$) above, which match with each other within an accuracy of 0.6%, indicating a consistency of the theory and a high precision of the numerics. We note that the systematic method of nonsymmorphic bosonization discussed in this section can be directly generalized to other 1D nonsymmorphic systems
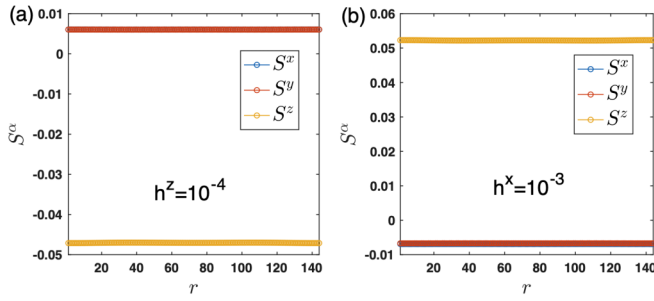
FIG. 4. Spin expectation values of S_r^α ($\alpha = x, y, z$) under uniform magnetic fields (a) $h^z = 10^{-4}$ along the z direction, (b) $h^x = 10^{-3}$, as functions of site r ($1 \leqslant r \leqslant 144$). The data of S^x and S^y nearly overlap, making the points of S^x hardly identifiable. DMRG simulations are performed for $K = 2.1$, $J = -1$, $\Gamma = 0.8$, on a system of $L = 144$ sites, using periodic boundary conditions.

including Kitaev ladders and doped Kitaev models, which is helpful for understanding more delicate structures previously ignored in those cases.

Response to magnetic field. With the ten extracted coefficients, Eq. (3) can be used to analytically calculate any desired low-energy property of the system. As an application of Eq. (3), we consider the response of the 1D $KJ\Gamma$ model to weak magnetic fields. By applying $(U_4)^{-1}$ to Eq. (3), it can be shown that at low energies, the coupling to a uniform weak magnetic field is given by $\sum_j \vec{h} \cdot \vec{S}_j = 4[h_C(h^x + h^y) + i_C h^z] \int dx N^z$. Since N^z is a relevant perturbation, a spin gap opens for an arbitrarily small uniform field, and the spin magnetization can be determined from Eq. (3) as $\langle \vec{S}_j \rangle = \langle N^z \rangle (h_C, h_C, i_C)$ in the unrotated frame. Interestingly, in this weak-field limit, the direction of the spin magnetization is fixed by h_c and i_c up to an overall sign and does not depend on the direction of the applied magnetic field. To verify this prediction, we study the response to magnetic fields using DMRG at a representative point $K = 2.1$, $J = -1$, $\Gamma = 0.8$. Figures 4(a) and 4(b) show $\langle \vec{S}_r \rangle$ as a function of r under uniform magnetic fields $h^z = 10^{-4}$ along the z direction and $h^x = 10^{-3}$ along the x direction, respectively. The extracted value $h_C/i_C = \langle S_r^x \rangle / \langle S_r^z \rangle$ is -0.128 (for h^z) and -0.130 (for h^x), which are consistent with each other.

2D zigzag order. As another application of Eq. (3), we derive the pattern of spin ordering for a system of weakly coupled 1D chains as shown in Fig. 1(a), which is a dimerized $KJ\Gamma$ model on the honeycomb lattice. The interaction on bond γ is $\alpha_\gamma [KS_i^\gamma S_j^\gamma + J\vec{S}_i \cdot \vec{S}_j + \Gamma(S_i^\alpha S_j^\beta + S_i^\beta S_j^\alpha)]$, where $\alpha_x = \alpha_y = 1$ and $\alpha_z \ll 1$. Using the nonsymmorphic bosonization formulas, the mean-field Hamiltonian in the four-sublattice rotated frame for the chain enclosed by the red dashed line in Fig. 1(a) can be derived as $H_{MF} = H_{LL} - \frac{\lambda}{a^3} \langle \cos(\sqrt{\pi}\theta) \rangle \int dx \cos(\sqrt{\pi}\theta)$, where H_{LL} is the Luttinger liquid Hamiltonian and $\lambda = |J|(a_C^2 + b_C^2) - (K + J)c_C^2 + 2\Gamma a_C b_C$. Since N^x and N^y have the smallest scaling dimension [both equal to $(4\kappa)^{-1}$], it is expected that the leading instability is in the $S^x S^y$ plane. Although different directions in the $S^x S^y$ plane in the Luttinger liquid theory are equivalent, the symmetry-allowed irrelevant term

$\cos(4\sqrt{\pi}\theta)$ stabilizes a spin order which satisfies the condition that one of $\langle N^\alpha \rangle$ ($\alpha = x, y$) does not vanish, but not both.

Assuming $\langle N^x \rangle \neq 0$, applying Eq. (3), and transforming back to the original frame, the spin expectation values are determined as $\vec{S}_{m,n} = \sqrt{2} \cos[\frac{\pi}{2}(n - m) + \frac{1}{2}] \langle N^x \rangle (a_C, -b_C, c_C)$, in which m and n are the row and column indices in the equivalent brick-wall lattice, respectively, and $m = 1$ for the enclosed chain in Fig. 1(a). The solid and open circles in Fig. 1(a) represent the sites which have positive and negative components along the S^x direction, respectively, and it can be seen that the pattern is exactly the 2D zigzag order, recovering the zigzag phase in the 2D $KJ\Gamma$ model [30,36]. However, we note that the spin orientations also contain components along the S^y and S^z directions as a consequence of Eq. (3). Furthermore, using the variational method for the massive sine-Gordon model [54] and solving the self-consistent mean-field equation, we obtain $\langle \cos(\sqrt{\pi}\theta) \rangle = [\pi\lambda/(v\kappa\Lambda^2 a^3)]^{\frac{1}{8\kappa - 2}}$ which determines the strength of the spin magnetization. Detailed discussions on weakly coupled chains are included in Sec. VI in SM [53].

Line of points with emergent $SU(2)_1$ symmetry. Finally, although the nonsymmorphic group is discrete and planar, we demonstrate that the phase boundary between the LL and FM phases in Fig. 2(a) has an emergent $SU(2)_1$ conformal symmetry [58]. The FM phase corresponds to a Néel order in the four-sublattice rotated frame with $\langle N^z \rangle \neq 0$ (see Sec. VII in SM [53]). Hence, at low energies, the phase transition between the LL and FM phases is the same as the easy-plane to easy-axis transition in the XXZ model, which is in the universality class described by the $SU(2)_1$ Wess-Zumino-Witten (WZW) model [59]. Instead of Abelian bosonization, the non-Abelian bosonization should be applied to the $SU(2)_1$ line, i.e., J^α and N^α ($\alpha = x, y, z$) in Eq. (3) should be replaced by the current operators and primary fields in the $SU(2)_1$ WZW theory, respectively. Nevertheless, the nonsymmorphic non-Abelian bosonization formulas on the $SU(2)_1$ line remain the same form as Eq. (3), still containing ten free coefficients. Numerical verifications of the emergent $SU(2)_1$ conformal symmetry are included in Sec. VII in SM [53].

In summary, we have derived the nonsymmorphic bosonization formulas for the spin-$\frac{1}{2}$ Kitaev-Heisenberg-Gamma model in the antiferromagnetic Kitaev region. The response to weak magnetic fields is analyzed, and the zigzag phase in the 2D model is obtained by weakly coupling an infinite number of chains. In addition, a line of critical points is found with emergent $SU(2)_1$ conformal symmetry in the phase diagram.

[1] C.-X. Liu, R.-X. Zhang, and B. K. VanLeeuwen, Phys. Rev. B **90**, 085304 (2014).

[2] C. Fang and L. Fu, Phys. Rev. B **91**, 161105(R) (2015).

[3] Z. Wang, A. Alexandradinata, R. J. Cava, and B. A. Bernevig, Nature (London) **532**, 189 (2016).

[4] A. Alexandradinata, Z. Wang, and B. A. Bernevig, Phys. Rev. X **6**, 021008 (2016).

[5] K. Shiozaki, M. Sato, and K. Gomi, Phys. Rev. B **93**, 195413 (2016).

[6] B. Bradlyn, J. Cano, Z. Wang, M. G. Vergniory, C. Felser, R. J. Cava, and B. A. Bernevig, Science **353**, aaf5037 (2016).

[7] P.-Y. Chang, O. Erten, and P. Coleman, Nat. Phys. **13**, 794 (2017).

[8] J. Ma, C. Yi, B. Lv, Z. Wang, S. Nie, L. Wang, L. Kong, Y. Huang, P. Richard, P. Zhang, K. Yaji, K. Kuroda, S. Shin, H. Weng, B. A. Bernevig, Y. Shi, T. Qian, and H. Ding, Sci. Adv. **3**, e1602415 (2017).

[9] B. Bradlyn, L. Elcoro, J. Cano, M. G. Vergniory, Z. Wang, C. Felser, M. I. Aroyo, and B. A. Bernevig, Nature (London) **547**, 298 (2017).

[10] H. C. Po, A. Vishwanath, and H. Watanabe, Nat. Commun. **8**, 50 (2017).

[11] B. J. Wieder, B. Bradlyn, Z. Wang, J. Cano, Y. Kim, H. D. Kim, A. M. Rappe, C. L. Kane, and B. A. Bernevig, Science **361**, 246 (2018).

[12] H. Watanabe, H. C. Po, and A. Vishwanath, Sci. Adv. **4**, eaat8685 (2018).

[13] F. Lu, B. Shi, and Y.-M. Lu, New J. Phys. **19**, 073002 (2017).

[14] R. Thorngren and D. V. Else, Phys. Rev. X **8**, 011040 (2018).

[15] G. Jackeli and G. Khaliullin, Phys. Rev. Lett. **102**, 017205 (2009).

[16] J. Chaloupka, G. Jackeli, and G. Khaliullin, Phys. Rev. Lett. **105**, 027204 (2010).

[17] Y. Singh and P. Gegenwart, Phys. Rev. B **82**, 064412 (2010).

[18] C. C. Price and N. B. Perkins, Phys. Rev. Lett. **109**, 187201 (2012).

[19] Y. Singh, S. Manni, J. Reuther, T. Berlijn, R. Thomale, W. Ku, S. Trebst, and P. Gegenwart, Phys. Rev. Lett. **108**, 127203 (2012).

[20] K. W. Plumb, J. P. Clancy, L. J. Sandilands, V. V. Shankar, Y. F. Hu, K. S. Burch, H. Y. Kee, and Y. J. Kim, Phys. Rev. B **90**, 041112(R) (2014).

[21] H.-S. Kim, V. V. Shankar, A. Catuneanu, and H.-Y. Kee, Phys. Rev. B **91**, 241110(R) (2015).

[22] S. M. Winter, Y. Li, H. O. Jeschke, and R. Valentí, Phys. Rev. B **93**, 214431 (2016).

[23] S.-H. Baek, S.-H. Do, K.-Y. Choi, Y. S. Kwon, A. U. B. Wolter, S. Nishimoto, J. van den Brink, and B. Buchner, Phys. Rev. Lett. **119**, 037201 (2017).

[24] I. A. Leahy, C. A. Pocs, P. E. Siegfried, D. Graf, S. H. Do, K. Y. Choi, B. Normand, and M. Lee, Phys. Rev. Lett. **118**, 187203 (2017).

[25] J. A. Sears, Y. Zhao, Z. Xu, J. W. Lynn, and Y. J. Kim, Phys. Rev. B **95**, 180411(R) (2017).

[26] A. U. B. Wolter, L. T. Corredor, L. Janssen, K. Nenkov, S. Schonecker, S. H. Do, K. Y. Choi, R. Albrecht, J. Hunger, T. Doert, M. Vojta, and B. Buchner, Phys. Rev. B **96**, 041405(R) (2017).

[27] J. Zheng, K. Ran, T. Li, J. Wang, P. Wang, B. Liu, Z.-X. Liu, B. Normand, J. Wen, and W. Yu, Phys. Rev. Lett. **119**, 227208 (2017).

[28] I. Rousochatzakis and N. B. Perkins, Phys. Rev. Lett. **118**, 147204 (2017).

[29] Y. Kasahara, T. Ohnishi, N. Kurita, H. Tanaka, J. Nasu, Y. Motome, T. Shibauchi, and Y. Matsuda, Nature (London) **559**, 227 (2018).

[30] J. G. Rau, E. K.-H. Lee, and H.-Y. Kee, Phys. Rev. Lett. **112**, 077204 (2014).

[31] K. Ran, J. Wang, W. Wang, Z.-Y. Dong, X. Ren, S. Bao, S. Li, Z. Ma, Y. Gan, Y. Zhang, J. T. Park, G. Deng, S. Danilkin, S.-L. Yu, J.-X. Li, and J. Wen, Phys. Rev. Lett. **118**, 107203 (2017).

[32] W. Wang, Z.-Y. Dong, S.-L. Yu, and J.-X. Li, Phys. Rev. B **96**, 115103 (2017).

[33] A. Catuneanu, Y. Yamaji, G. Wachtel, Y. B. Kim, and H.-Y. Kee, npj Quantum Mater. **3**, 23 (2018).

[34] M. Gohlke, G. Wachtel, Y. Yamaji, F. Pollmann, and Y. B. Kim, Phys. Rev. B **97**, 075126 (2018).

[35] X. Liu, T. Berlijn, W.-G. Yin, W. Ku, A. Tsvelik, Y.-J. Kim, H. Gretarsson, Yogesh Singh, P. Gegenwart, and J. P. Hill, Phys. Rev. B **83**, 220403(R) (2011).

[36] J. Chaloupka, G. Jackeli, and G. Khaliullin, Phys. Rev. Lett. **110**, 097204 (2013).

[37] R. D. Johnson, S. C. Williams, A. A. Haghighirad, J. Singleton, V. Zapf, P. Manuel, I. I. Mazin, Y. Li, H. O. Jeschke, R. Valentí, and R. Coldea, Phys. Rev. B **92**, 235119 (2015).

[38] Y. Motome, R. Sano, S. H. Jang, Y. Sugita, and Y. Kato, J. Phys.: Condens. Matter **32**, 404001 (2020).

[39] A. Kitaev, Ann. Phys. **321**, 2 (2006).

[40] C. Nayak, S. H. Simon, A. Stern, M. Freedman, and S. Das Sarma, Rev. Mod. Phys. **80**, 1083 (2008).

[41] C. E. Agrapidis, J. van den Brink, and S. Nishimoto, Sci. Rep. **8**, 1815 (2018).

[42] C. E. Agrapidis, J. van den Brink, and S. Nishimoto, Phys. Rev. B **99**, 224418 (2019).

[43] A. Catuneanu, E. S. Sørensen, and H.-Y. Kee, Phys. Rev. B **99**, 195112 (2019).

[44] W. Yang, A. Nocera, T. Tummuru, H.-Y. Kee, and I. Affleck, Phys. Rev. Lett. **124**, 147205 (2020).

[45] W. Yang, A. Nocera, and I. Affleck, Phys. Rev. Res. **2**, 033268 (2020).

[46] W. Yang, A. Nocera, and I. Affleck, Phys. Rev. B **102**, 134419 (2020).

[47] W. Yang, A. Nocera, E. S. Sørensen, H.-Y. Kee, and I. Affleck, Phys. Rev. B **103**, 054437 (2021).

[48] W. Yang, A. Nocera, P. Herringer, R. Raussendorf, and I. Affleck, Phys. Rev. B **105**, 094432 (2022).

[49] Q. Luo, J. Zhao, X. Wang, and H.-Y. Kee, Phys. Rev. B **103**, 144423 (2021).

[50] Q. Luo, S. Hu, and H.-Y. Kee, Phys. Rev. Res. **3**, 033048 (2021).

[51] Z.-A. Liu, T.-C. Yi, J.-H. Sun, Y.-L. Dong, and W.-L. You, Phys. Rev. E **102**, 032127 (2020).

[52] E. S. Sørensen, A. Catuneanu, J. S. Gordon, and H.-Y. Kee, Phys. Rev. X **11**, 011013 (2021).

[53] See Supplemental Material at http://link.aps.org/supplemental/10.1103/PhysRevB.109.L180403 for which contains discussions on nonsymmorphic symmetry group of the system, derivation of the nonsymmorphic bosonization formulas, numerical method for fitting correlation functions, response to

external magnetic fields, analysis of weakly coupled chains, and numerical results on the line of emergent $SU(2)_1$ conformal symmetry.

[54] T. Giamarchi, *Quantum Physics in One Dimension* (Clarendon, Oxford, UK, 2004).

[55] I. Affleck, in *Fields, Strings and Critical Phenomena, Proceedings of Les Houches Summer School, 1988*, edited by E. Brezin and J. Zinn-Justin (North-Holland, Amsterdam, 1990), pp. 563–640.

[56] The normalizations of J^α and N^α are chosen such that their correlation functions are normalized in a way shown in Sec. III B in SM [53].

[57] In all DMRG simulations in this Letter, the bond dimension m and truncation error ϵ are taken as $m = 1400$ and $\epsilon = 10^{-9}$.

[58] This analysis integrates the phase diagram of the spin-$\frac{1}{2}$$KJ\Gamma$ chain obtained in Ref. [44], where this line of critical points with emergent $SU(2)_1$ symmetry was not found.

[59] Indeed, as can be seen from Eq. (2), when $K + 2J = 0$, the system is SU(2) invariant at long distances regardless of the value of Γ, since the Γ term vanishes when the neighboring sites can no longer be distinguished. Higher-order effects shift the location of the phase transition line, but the emergent $SU(2)_1$ symmetry is expected to persist.